

# Development of spatiotemporal receptive fields of simple cells: II. Simulation and analysis

S. Wimbauer<sup>1</sup>, O. G. Wenisch<sup>1</sup>, J. L. van Hemmen<sup>1</sup>, K. D. Miller<sup>2</sup>

<sup>1</sup> Physik Department, Technische Universität München, D-85747 Garching, Germany

<sup>2</sup> Departments of Physiology and Otolaryngology, W. M. Keck Foundation Center for Integrative Neuroscience, Sloan Center for Theoretical Neurobiology, University of California, San Francisco, CA 94143-0444, USA

Received: 18 June 1997 / Accepted: 16 September 1997

**Abstract.** In part I of this article a correlation based model for the developmental process of spatiotemporal receptive fields has been introduced. In this model the development is described as an activity-dependent competition between four types of input from the lateral geniculate nucleus onto a cortical cell, viz. non-lagged ON and OFF and lagged ON and OFF inputs. In the present paper simulation results and a first analysis are presented for this model. We study the developmental process both before and after eye-opening and compare the results with experimental data from reverse correlation measurements. The outcome of the developmental process is determined mainly by the spatial and the temporal correlations between the different inputs. In particular, if the mean correlation between non-lagged and lagged inputs is weak, receptive fields with a widely varying degree of direction selectivity emerge. However, spatiotemporal receptive fields may show rotation of their preferred orientation as a function of response delay. Even if the mean correlation between two types of temporal input is not weak, direction-selective receptive fields may emerge because of an intracortical interaction between different cortical maps. In an environment of moving lines or gratings, direction-selective receptive fields develop only if the distribution of the directions of motion presented during development shows some anisotropy. In this case, a continuous map of preferred direction is also shown to develop.

## 1 Introduction

In the preceding paper [27] we derived a model for the development of spatiotemporal receptive fields of cortical simple cells. According to this model the development is driven by spatiotemporal correlations between four types of input from the lateral geniculate nucleus (LGN) onto a cortical cell, viz. lagged and non-lagged ON and OFF inputs. The development can be described by the following central equation:

Correspondence to: J.L. van Hemmen  
(e-mail: lvh@physik.tu-muenchen.de)

$$\begin{aligned} \frac{dJ^{c,\tau}(\mathbf{x}, \boldsymbol{\alpha}, t)}{dt} &= \lambda A(\mathbf{x} - \boldsymbol{\alpha}) \sum_{\mathbf{x}'} I(\mathbf{x}, \mathbf{x}') \\ &\times \sum_{c'=ON, OFF} \sum_{\tau'=nl, l} \sum_{\boldsymbol{\alpha}''} C^{c,c';\tau,\tau'}(\boldsymbol{\alpha}, \boldsymbol{\alpha}'') J^{c',\tau'}(\mathbf{x}', \boldsymbol{\alpha}'', t) \\ &- \epsilon(\mathbf{x}) A(\mathbf{x} - \boldsymbol{\alpha}), \end{aligned} \quad (1)$$

where  $c$  stands for ON or OFF,  $\tau$  for non-lagged or lagged, while

$$\epsilon(\mathbf{x}) = \frac{\left[ \sum_{\boldsymbol{\alpha}'} \sum_{c=ON, OFF} \sum_{\tau=nl, l} \left. \frac{d}{dt} \right|_u J^{c,\tau}(\mathbf{x}, \boldsymbol{\alpha}', t) \right]}{4 \sum_{\boldsymbol{\alpha}'} A(\mathbf{x} - \boldsymbol{\alpha}')}, \quad (2)$$

and  $\left. \frac{d}{dt} \right|_u J^{c,\tau}(\mathbf{x}, \boldsymbol{\alpha}')$  is given by the first two lines of (1). Furthermore, the growth of the synapses is limited by upper and lower bounds,

$$0 \leq J^{c,\tau}(\mathbf{x}, \boldsymbol{\alpha}) \leq J_{\max} A(\mathbf{x} - \boldsymbol{\alpha}). \quad (3)$$

All functions used in the above equations have been introduced in [27]. In particular, spatiotemporal correlation functions both for development before and after eye-opening have been derived there. In the present paper we explore different scenarios for the competition between the four types of spatiotemporal input from the LGN. In doing so, we demonstrate in numerical simulations and in a first analysis that the emergence of spatiotemporal receptive field properties, in particular direction selectivity, can be understood in the framework of activity-dependent learning. We will also clarify the conceptual limitations that arise in a purely linear developmental model as is studied here. In the first three scenarios, we consider competition based on unstructured spontaneous activity, as might be typical during development before eye-opening. Uncorrelated noise in the photoreceptors is filtered through the lagged and non-lagged spatiotemporal receptive fields, resulting in correlations that depend on certain parameters specifying those receptive fields. If the mean correlation between lagged and non-lagged inputs to the cortical cell is weak, a whole range of spatiotemporal receptive fields with different degrees of direction selectivity can be observed, and the distribution of direction selectivities agrees well with that observed in reverse-correlation experiments [3, 4]. However, the preferred orientations of the lagged and non-lagged inputs to a cell are then uncorrelated,

resulting in spatiotemporal receptive fields whose preferred orientation changes with time. Experimentally, this feature of a spatiotemporal receptive field appears to be uncommon, at least in adult animals [2, 3, 26], although some authors report receptive fields with preferred orientations that drift over time [21, 24]. If the correlations between lagged and non-lagged inputs are stronger, then the preferred orientations of the two types of input coincide but direction selectivity fails to develop. We also demonstrate that simple *intracortical* connections can result in spatiotemporal receptive fields that are sensitive to the direction of motion, even if the correlation between the two types of temporal input is not weak. Again, this scenario produces spatiotemporal receptive fields with preferred orientations that rotate with time. We then consider a fourth scenario in which direction selectivity arises from development in an environment of moving lines or gratings, as might arise due to patterned vision and/or from spindle waves traversing the LGN during sleep [11, 16]. We begin by studying the developmental process assuming that patterns with only one particular direction of motion occur as input. Such activity patterns lead to mature receptive fields with both direction and orientation selectivities similar to those observed experimentally. However, for the general case of arbitrary directions of motion, direction selective receptive fields develop in our model only if some anisotropy remains in the distribution of the directions of motion that are presented during development. Feidler et al. [7] have studied how nonlinearities that suppress plasticity when the postsynaptic cell is poorly activated can increase competition and allow direction selectivity to emerge from isotropic input; we will return to this in the Discussion.

The paper is organized as follows. In Sect. 2 the details of the simulation algorithm and the methods to derive and analyze spatiotemporal receptive fields are described. Simulation results of our model for four different scenarios, including assumptions of either unstructured or structured input activity, are presented in Sect. 3. A simple analysis that explains the basic reasons for these simulation results is presented in Sect. 4. We conclude our considerations with a discussion of the results in Sect. 5.

## 2 Methods

### 2.1 Architecture of the network model and simulation algorithm

To study the behavior of our developmental system in numerical simulations we model cortical simple cells, non-lagged ON and OFF inputs, and lagged ON and OFF inputs from the LGN by five square grids of the *same* size where the retinotopic positions on all grids correspond to each other. The number of neurons in each grid is  $32 \times 32$  or  $23 \times 23$ , depending on the simulation. Each cortical cell receives inputs from all four types of LGN cells. These input neurons lie within a circle centered at the retinotopic position of the cortical cell. The diameter of the circle is chosen so as to extend over 13 or 11 neurons, depending on the simulation. Periodic boundary conditions have been applied throughout.

The simulation algorithm proceeds along the same steps as the ones used by Miller [18]. A more detailed description of the algorithm can be found there. All four types of synapse have been assigned random initial values uniformly distributed over  $(1 \pm s_{\text{noise}})A(\mathbf{x} - \boldsymbol{\alpha})$  with  $s_{\text{noise}} = 0.2$ .

During each timestep of the simulation, the change in synaptic strength  $\frac{d}{dt}\big|_{\text{u}} J^{c,\tau}(\mathbf{x}, \boldsymbol{\alpha}')$  is calculated according to the first two lines of (1). If the temporal correlation function, cf. (16) in [27], is independent of the position  $\boldsymbol{\alpha}$  of the neuron in the LGN, the change in synaptic strength  $\frac{d}{dt}\big|_{\text{u}} J^{c,\tau}(\mathbf{x}, \boldsymbol{\alpha}')$  can be calculated using Fourier transforms, as described in [18]. In this case a grid size of  $32 \times 32$  neurons and an arbor diameter of 13 have been used. On the other hand, if the form of the lagged response and hence the temporal correlation depends on  $\boldsymbol{\alpha}$ ,  $\frac{d}{dt}\big|_{\text{u}} J^{c,\tau}(\mathbf{x}, \boldsymbol{\alpha}')$  has to be calculated directly. This needs more computer time. Accordingly, smaller grid and arbor sizes have to be used, in particular, a size of 23 for the grid and an arbor diameter of 11.

In most simulations the growth constant  $\lambda$  has been adjusted in such a way that the standard deviation for the change in synaptic strength becomes 0.005 or 0.01 for the first time step, depending on whether or not a spatially homogeneous network is used. This corresponds to a value for  $\lambda$  of about 0.01 or 0.02. For some simulations we have tested an even smaller growth constant  $\lambda$ , resulting in a standard deviation of only 0.0025. Simulation results have not been affected by lowering the growth constant in this way.

After the change in the synaptic strength,  $\frac{d}{dt}\big|_{\text{u}} J^{c,\tau}(\mathbf{x}, \boldsymbol{\alpha}')$ , has been calculated, the result is subjected to the constraints described in (2). If any of the synapses  $J^{c,\tau}(\mathbf{x}, \boldsymbol{\alpha})$  falls below the lower bound 0 or rises above the upper bound  $J_{\text{max}}A(\mathbf{x} - \boldsymbol{\alpha})$ , the values are cut off at zero or  $J_{\text{max}}A(\mathbf{x} - \boldsymbol{\alpha})$ , respectively. Once cut off, a synapse is “frozen”: it is thereafter assigned unconstrained derivative zero, and the sums in both numerator and denominator in the definition of  $\epsilon(\mathbf{x})$  (cf. Eq. 2) are thereafter restricted to combinations  $\{c, \tau, \boldsymbol{\alpha}', \mathbf{x}\}$  that correspond to active (unfrozen) synapses. To correct for the cutoff and to ensure that the total synaptic strength received by one cortical cell remains fixed at  $4 \sum_{\boldsymbol{\alpha}} A(\mathbf{x} - \boldsymbol{\alpha})$ , immediately after the cutoffs all active synapses are multiplied by  $\gamma(\mathbf{x}) = [4 \sum_{\boldsymbol{\alpha}} A(\mathbf{x} - \boldsymbol{\alpha}) - J_{\text{frozen}}(\mathbf{x})]/J_{\text{active}}(\mathbf{x})$ . Here,  $J_{\text{frozen}}(\mathbf{x})$  and  $J_{\text{active}}(\mathbf{x})$  are the sums over  $\{c, \tau, \boldsymbol{\alpha}'\}$  corresponding to frozen and active synapses, respectively, of  $J^{c,\tau}(\mathbf{x}, \boldsymbol{\alpha}')$ .  $\gamma(\mathbf{x})$  is restricted to  $0.8 \leq \gamma(\mathbf{x}) \leq 1.2$ .

The simulation was stopped if more than 90% of the synapses had reached their upper and lower bounds. This took between 20 and 160 timesteps.

### 2.2 Derivation of spatiotemporal receptive fields and calculation of receptive field properties

As an outcome of a simulation, we obtain the synaptic weights of the four types of input from the LGN, i.e., non-lagged and lagged ON and OFF inputs. We now have to clarify how the spatiotemporal receptive field profiles are derived from these synaptic weights. All steps in deriving and analyzing the spatiotemporal receptive fields have been chosen in such a way that they mimic as closely as possi-

ble the approach taken in reverse correlation measurements; cf. [3].

The response of a simple cell and hence its receptive field is given by the sum of the different spatiotemporal channels weighted by the synapses; cf. (2) in [27]. This sum is convolved subsequently with the intracortical interaction function.

To be more specific, we now consider a simple cell at a cortical position  $\mathbf{x}$  that receives input from neurons in the LGN within an arbor of radius  $D_A/2$ . In order to obtain the receptive field of this cell, the temporal response profiles for non-lagged and lagged inputs are multiplied by their synaptic weights  $J^{c,\tau}(\mathbf{x}, \boldsymbol{\alpha})$  and added up for each relevant LGN position  $\boldsymbol{\alpha}$ . Then the resulting quantities for ON- and OFF-type inputs are subtracted. This corresponds to subtracting the response profiles for dark and bright spots in a reverse correlation measurement, as described in [27], Sect. 2.

It should be mentioned that we neglect the effects of the center-surround profile  $R^c(\boldsymbol{\alpha} - \boldsymbol{\alpha}')$ , which would result in a slight smoothing of the spatial receptive field profiles but does not change the spatial pattern of the receptive field. This approximation has been discussed elsewhere [18].

A further convolution of the receptive field profile with the intracortical interaction function is performed only in those simulations where the form of the lagged response does not depend on the LGN position  $\boldsymbol{\alpha}$ . The only effect of including cortical interactions on the receptive field profile was to widen the spatial receptive field slightly.

In most cases one is interested in the response of the cell to stimuli that are oriented along the preferred orientation of the receptive field. We have therefore integrated the spatiotemporal receptive field along its preferred orientation. When a spatiotemporal receptive field is displayed in this article the temporal axis and the spatial axis *perpendicular* to the preferred orientation are shown. This approach is consistent with the reverse correlation study of DeAngelis et al. [3].

The response of a cell to a drifting sine wave grating can now be derived easily with our assumption of linear response, for the case of a grating with wave front parallel to the preferred orientation of the cell. To this end, the Fourier transform of the two-dimensional (i.e. integrated along the preferred orientation) spatiotemporal receptive field is calculated. The amplitude of the Fourier transform for a wave-vector  $(k, \omega)$  is now equivalent to the peak response of the cell to a grating with a spatial frequency  $k$  moving at a speed  $v = \omega/k$ .

Following DeAngelis et al. [3], a *direction selectivity index* (DSI) is defined that characterizes the difference in response of a sine wave grating for right- and leftward motion:

$$\text{DSI} = \frac{R_p - R_n}{R_p + R_n}. \quad (4)$$

$R_p$  and  $R_n$  are the maximum amplitudes of the Fourier transform within the first and second quadrant of the  $k$ - $\omega$  plane, respectively.  $R_p$  corresponds to the peak response for rightward motion of the sine wave grating and  $R_n$  to the peak response for leftward motion. In this way a positive direction selectivity index signals a preference of the cell for stimuli moving rightward, and vice versa.

The preferred orientation and orientation selectivity have been derived in a similar way to [18]. First, the amplitude of the Fourier transform  $|J^{\text{ON},\tau}(\mathbf{x}, \mathbf{k}) - J^{\text{OFF},\tau}(\mathbf{x}, \mathbf{k})|$  of  $J^{\text{ON},\tau}(\mathbf{x}, \boldsymbol{\alpha}) - J^{\text{OFF},\tau}(\mathbf{x}, \boldsymbol{\alpha})$  is calculated for  $\tau \in \{\text{nl}, 1\}$  separately. This corresponds to the peak response of a cell to a stationary sine wave grating with wave vector  $\mathbf{k}$  for the non-lagged and the lagged inputs alone. Subsequently, the best response over all wave vectors  $\mathbf{k}$  in each  $10^\circ$  interval between  $0^\circ$  and  $180^\circ$  is evaluated. This defines a function  $R^\tau(\mathbf{x}, n)$  for  $n = 0, \dots, 17$  and  $\tau \in \{\text{nl}, 1\}$ . For the  $n^{\text{th}}$  interval, a 2-D vector is constructed with length  $R^{\text{nl}}(\mathbf{x}, n) + R^1(\mathbf{x}, n)$  and angle  $n \times 20^\circ$ . The vector sum of these 18 vectors gives a vector  $\nu_R(\mathbf{x})$ , with length  $|\nu_R(\mathbf{x})|$ . The preferred orientation is defined as the angle of this vector divided by 2 and orientation selectivity as the ratio of  $|\nu_R(\mathbf{x})|/18$  to the root mean square length of the 18 individual vectors.

In order to evaluate how orientation selectivity is modified by combining lagged and non-lagged inputs, this quantity is also calculated for non-lagged and lagged inputs separately. This is done by assigning a length  $R^{\text{nl}}(\mathbf{x}, n)$  or  $R^1(\mathbf{x}, n)$  instead of  $R^{\text{nl}}(\mathbf{x}, n) + R^1(\mathbf{x}, n)$  to the vector of the  $n^{\text{th}}$  interval. All other steps are performed in the same way as described above.

### 3 Results: simulations

In this section the simulation results of our model are presented for four different scenarios. The first three scenarios describe the case where uncorrelated noise in the photoreceptors drives the development, as might be typical for a development before eye-opening. The correlation function for this case has been derived in [27], Sect. 3. In the first scenario (Sect. 3.1), the temporal response functions of non-lagged and lagged inputs are *the same* for all input channels. This scenario is particularly suitable for the study of the basic mechanisms underlying our model. In the second scenario (Sect. 3.2), the form of the lagged response depends in a *random* way on the position  $\boldsymbol{\alpha}$  of the input cell on the LGN grid, which seems to be more realistic for a biological system. In a third scenario (Sect. 3.3), we demonstrate how *intracortical* connections can cause a direction-selective response, even if the weight distribution from the LGN to the cortex is spatiotemporally separable and, hence, does not give rise to a direction-selective receptive field by itself. In the fourth scenario (Sect. 3.4), we study the development of direction selectivity in an environment of *moving* patterns. The corresponding correlation function has also been calculated in [27], Sect. 3.

#### 3.1 Constant correlations between non-lagged and lagged inputs

The outcomes of two typical simulation runs for the first scenario are shown in Figs. 1 and 3. In Fig. 1 the constant  $f_s$  that determines the form of the lagged response function has been chosen to be  $f_s = 8.5$  Hz; cf. (8) in [27]. This results in a weak negative correlation between the two types of temporal input channels:  $\text{corr} = -0.05$ , using (20) in [27] which corresponds to the case of noise-driven development.

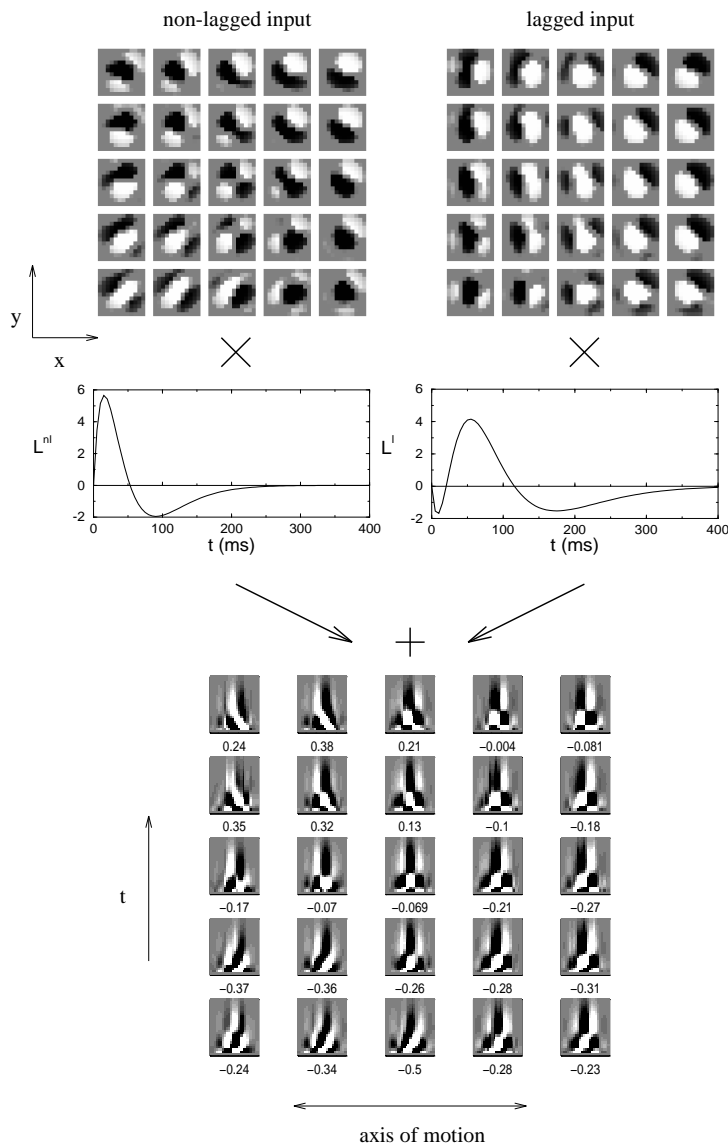


**Fig. 1.** A  $5 \times 5$  detail from a grid of  $32 \times 32$  cortical neurons is displayed for a simulation of scenario I with *weak* correlations between non-lagged and lagged inputs ( $f_s = 8.5$  Hz or  $\text{corr} = -0.05$ ). The spatial receptive fields for non-lagged and lagged inputs are shown separately in the first line. These spatial receptive fields are obtained by subtracting OFF from ON synaptic weights. Due to the low correlation between the two types of temporal input, the non-lagged and lagged orientation maps develop nearly independently, and the non-lagged and lagged spatial receptive fields of one cortical cell can have different phases and orientations. This results in spatiotemporally non-separable receptive fields that are direction-selective, as shown, e.g., in the bottom line. Spatiotemporal receptive fields are calculated by multiplying the spatial receptive fields of non-lagged and lagged inputs by their respective temporal response function, adding them, and integrating the result along the axis of preferred orientation. The direction selectivity index as defined by (4) can be found underneath each spatiotemporal receptive field

In the top line of Fig. 1 the difference between ON and OFF inputs is displayed for a  $5 \times 5$  detail of the whole  $32 \times 32$  grid for non-lagged and lagged channels. Each of the small squares corresponds to one cortical cell and shows the distribution of synaptic weights that link this cell with cells in the LGN that are located in a  $13 \times 13$  grid centered at the retinotopic position of the cortical cell. A single square thus corresponds to the cell's spatial receptive field, split into non-lagged and lagged inputs. White denotes positive values or predominantly ON inputs, black indicates negative values or predominantly OFF inputs.

The spatial receptive fields formed by non-lagged or lagged inputs alone each develop an orientation map. By *orientation map*, we mean that the ON and OFF inputs form elongated subregions within the receptive field of each cortical cell, the orientation of which varies fairly continuously from cell to cell. The phase of these receptive fields also varies. The notion of the *phase* of a spatial receptive field goes back to the modeling of simple cell receptive fields by Gabor functions, that is, by functions of the form  $J(\alpha) = \exp(-|\alpha|^2/(2A)) \cos(k \cdot \alpha + \theta)$  [10]. Accordingly,

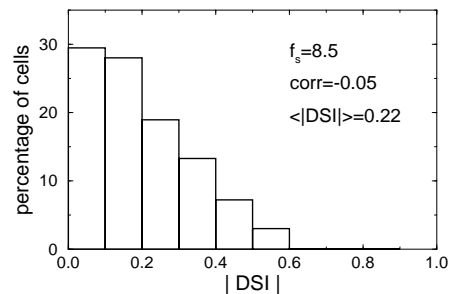


**Fig. 2.** Distribution of the absolute value of the direction selectivity index for a simulation run with  $f_s = 8.5$  Hz, which corresponds to a weak negative correlation between non-lagged and lagged inputs of  $\text{corr}(f_s) = -0.05$ . The distribution resembles closely the distribution of  $|\text{DSI}|$  obtained from reverse correlation measurements as presented in [3]

for phase 0 an ON or OFF subregion is centered in the middle of the receptive field, whereas for a phase of  $\pi/2$  ON and OFF subregions of the same size form the right and the left half of the receptive field. The question of what types

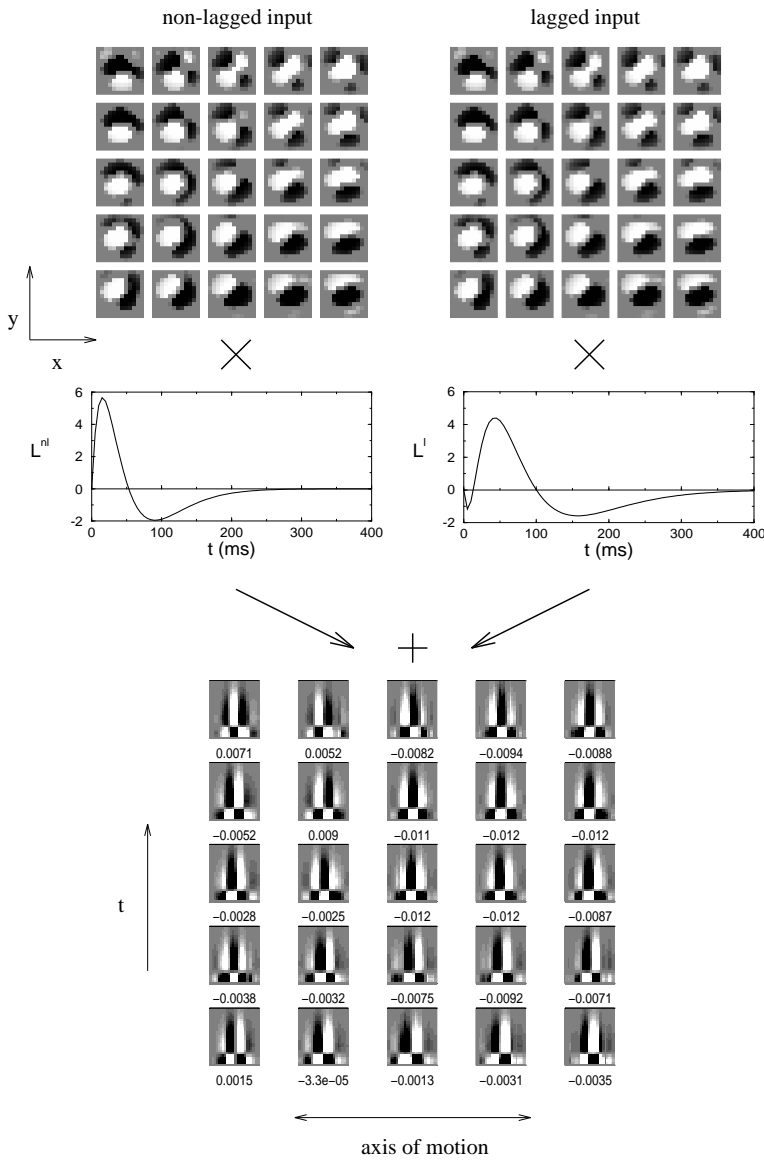


**Fig. 3.** The same subplots as in Fig. 1 are shown, but now for *strong* correlations between non-lagged and lagged inputs; here  $f_s = 15.3$  Hz corresponding to  $\text{corr}(15.3) = 0.3$ . The spatial orientation maps for non-lagged and lagged inputs are nearly identical. Hence the resulting spatiotemporal receptive fields are all spatiotemporally separable and the direction selectivity of all cells is weak

of orientation maps develop in which parameter regime has already been discussed in great detail elsewhere [18].

Since the activity correlation between non-lagged and lagged inputs is very weak, and each develops from different (random) initial conditions, the maps of lagged and non-lagged inputs develop nearly independently. Hence, the orientation and the phase of the non-lagged and lagged spatial receptive field of *one* cortical cell will be nearly uncorrelated.

To obtain a spatiotemporal receptive field, the spatial receptive fields for the two temporal input types are multiplied by their respective temporal response function and then added, as described in the previous section. In the third row of Fig. 1, the spatiotemporal receptive fields are displayed after an integration along the preferred orientation (this preferred orientation is the orientation of a grating stimulus that yields maximum combined non-lagged and lagged input to the cell; it need not correspond to the preferred orientation of either the non-lagged or lagged inputs alone). The direction selectivity index of each cell can be found underneath the receptive field.

A good example of a cell that shows strong direction selectivity is the one in the center of the bottom row. The ON and OFF subregions are tilted clockwise in the  $x$ - $t$  plane. The cell therefore responds better to leftward than to rightward motion; cf. Fig. 1 in [27]. If one goes back to the respective spatial receptive fields of the lagged and the non-lagged inputs, one notices that the non-lagged input has a phase of about  $\pi/2$ , whereas the lagged input has approximately zero phase. We will demonstrate later on in more detail that a difference in phase between the lagged and non-lagged inputs is an *essential* prerequisite for the emergence of a direction-selective response to an elongated stimulus.

In contrast, for example the spatiotemporal receptive field in the top right corner is nearly spatiotemporally separable. That is, it can be described by the product of a spatial and a temporal response function. This type of receptive field responds equally well to rightward and leftward motion, as is indicated by the low direction selectivity index of  $-0.081$ . The corresponding spatial receptive fields for non-lagged and lagged inputs *both* have a phase near  $\pm\pi/2$ . This example demonstrates that a whole range of spatiotemporal receptive

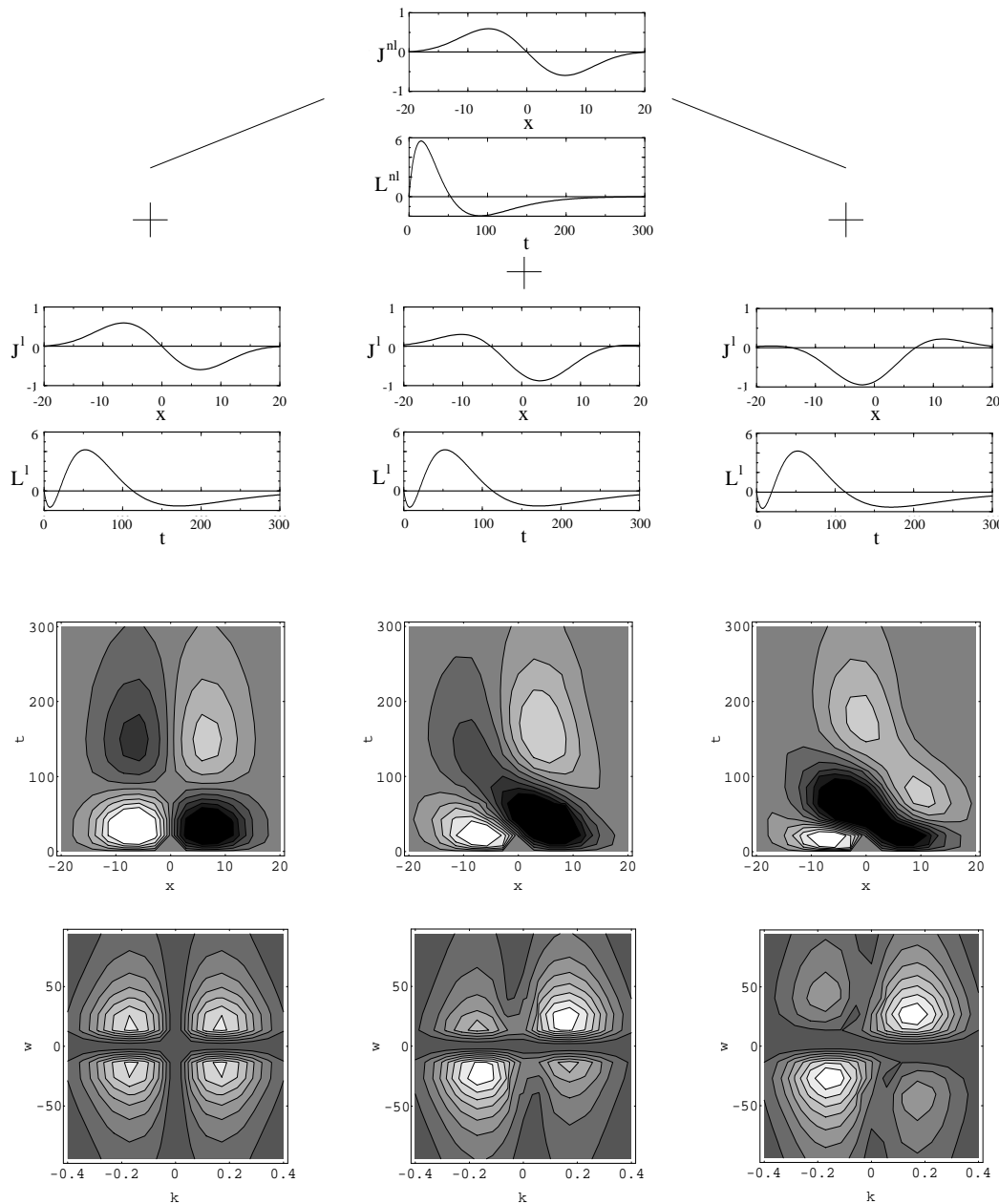


**Fig. 4.** The spatial receptive fields for non-lagged and lagged channels have been modeled by Gabor functions. A non-lagged input with a spatial phase of  $\theta_{nl} = 90^\circ$  is combined with a lagged input of either  $\theta_l = 90^\circ$ ,  $\theta_l = 135^\circ$ , or  $\theta_l = 210^\circ$  (from left to right). The spatial receptive fields ( $nl$  and  $l$ ), integrated along the axis of preferred orientation, and the respective temporal response functions are shown in the first two double-rows; cf. (5). In the third and fourth row, the resulting spatiotemporal receptive fields and a contour plot of the amplitudes of their Fourier transforms are displayed. The direction selectivity index increases from left to right, as becomes obvious from a growing difference in the peak amplitude of the Fourier transform between the first and the second quadrant. We have assigned the values  $A = 64$  and  $K = 0.15$  to the parameters of the Gabor functions according to (5). Furthermore, we have taken a value of 9.2 Hz for the parameter  $f_s = \omega_s/(2\pi)$  of the lagged response function

fields with different degrees of direction selectivity emerges if there is only a weak correlation between the two types of temporal input channels.

We have plotted the corresponding distribution of the absolute value of the direction selectivity index in Fig. 2. This histogram can be compared with the distribution of the quantity that one obtains from reverse correlation measurements. There is good agreement between this and Fig.17c of DeAngelis et al. [3], i.e. between experiment and model prediction.

However, there appears to be a problem in this scenario. Since non-lagged and lagged synapses are growing nearly independently, both types of temporal input not only develop different spatial phases, resulting in a direction-selective receptive field, but also different preferred orientations. The second cell from the left in the first row of the bottom pic-

ture of Fig. 1 may serve as an example of this case. Different orientations of non-lagged and lagged inputs correspond to a rotation of the preferred orientation in time, a feature that is rarely seen in simple cell responses [2, 3, 26], although some reports support the hypothesis of preferred orientation drifting in time [21, 24].

We now turn to Fig. 3 where the constant that determines the form of the lagged response has been taken to be  $f_s = 15.3$  Hz. In this case the correlation between non-lagged and lagged channels becomes  $\text{corr}(15.3) = 0.3$ . Again the top row of Fig. 3 shows the orientation map for non-lagged and lagged inputs separately. Because of the correlation between the two types of channel, the non-lagged and lagged maps are nearly identical and agree both in orientation and phase for each cortical cell. Hence, the resulting spatiotemporal

receptive fields are all spatiotemporally separable and show only very weak direction selectivity.

To investigate more closely what factors determine the direction selectivity of a simple cell in our model, we will now approximate the spatial receptive fields of non-lagged and lagged inputs by Gabor functions and vary the phase and orientation of these functions systematically. If a bar is presented as a stimulus, the spatial receptive fields and hence the Gabor functions  $J(\alpha) = \exp(-|\alpha|^2/(2A)) \cos(\mathbf{K}_\tau \cdot \alpha + \theta_\tau)$  have to be integrated along the orientation of the stimulus and one obtains

$$J^\tau(\alpha) = \sqrt{2\pi A} \exp\left(-\frac{\alpha^2}{2A}\right) \cos(K\alpha + \theta_\tau) \quad (5)$$

with  $\tau \in \{\text{nl}, \text{l}\}$ , where we have assumed that the bar is oriented parallel to the preferred orientation along the  $\beta$ -axis. It should be noted that the phases of the Gabor functions are not affected by the integration.

Figure 4 shows three examples in which a non-lagged input with a spatial phase of  $\theta_{\text{nl}} = 90^\circ$  is combined with a lagged input with either the same phase, a phase of  $\theta_{\text{l}} = 135^\circ$ , or a phase of  $\theta_{\text{l}} = 210^\circ$ .

In the first two rows of Fig. 4, the integrated spatial receptive fields and the temporal response functions for lagged and non-lagged inputs are displayed. The third and fourth lines show the resulting spatiotemporal receptive fields and the amplitudes of their Fourier transforms. For  $\theta_{\text{nl}} = \theta_{\text{l}} = 90^\circ$ , the receptive field is spatiotemporally separable, the amplitude of the Fourier transform is symmetric with respect to the  $k$ -axis<sup>1</sup>, and hence the cell responds in the same way to a bar moving rightward or leftward. For phases  $\theta_{\text{l}} = 135^\circ$  and  $\theta_{\text{l}} = 210^\circ$ , one can observe a growing difference between the amplitudes in the first and second quadrant of the Fourier transform, corresponding to an increase in the direction selectivity index.

In Fig. 5, the dependence of the direction selectivity index upon the difference between the lagged and the non-lagged phase of the Gabor functions is displayed for a non-lagged spatial phase  $\theta_{\text{nl}} = 90^\circ$ . To be consistent with our analysis of the receptive fields that stem from the developmental model, direction selectivity has been evaluated numerically for this plot. The direction selectivity index grows with increasing phase difference up to a maximum at  $\theta_{\text{l}} - \theta_{\text{nl}} \approx 120^\circ$ , and decreases thereafter.

To summarize, the emergence of direction selectivity is caused by a *difference in spatial phase* and not orientation for the non-lagged and lagged inputs. The phase difference that leads to a maximum direction selectivity index depends on the exact form of the temporal response functions and the spatial receptive field profiles. In the scenario under consideration this phase difference is due to a (nearly) independent development of the spatial map for the non-lagged and the lagged inputs, but comes at the cost of uncorrelated orientation maps for the two input types and hence preferred orientations that rotate with time.

We now investigate in more detail how the outcome of the simulations depends on the correlation between non-lagged and lagged inputs. In Fig. 6 the mean direction se-

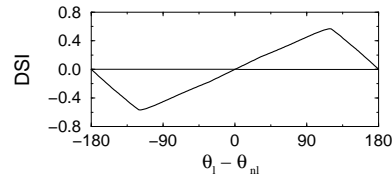


**Fig. 5.** The direction selectivity index (DSI) has been plotted against the spatial phase difference between lagged and non-lagged inputs. The spatial receptive fields for the two types of temporal input have been modeled by Gabor functions. The parameters of the Gabor functions and the lagged response function have been chosen as in Fig. 4. It can be recognized that for a linear model of direction selectivity a maximum value of  $\text{DSI} \approx 0.6$  can be obtained

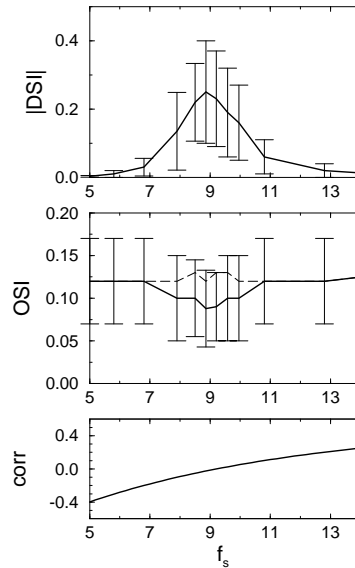


**Fig. 6.** The mean direction selectivity index (DSI) and the mean orientation selectivity index (OSI), together with their standard deviations, have been plotted as a function of  $f_s$ . The parameter  $f_s$  determines the form of the lagged response function and hence the correlation between non-lagged and lagged inputs, as is shown in the bottom graph. The average is performed over all  $32 \times 32$  cortical neurons of one simulation run. The *dashed curve* in the center graph displays the OSI for lagged inputs alone

lectivity index (DSI) and the mean orientation selectivity index (OSI), as defined in Sect. 2.2, have been plotted for various values of the parameter  $f_s$ . This parameter determines the functional form of the lagged response and hence the temporal correlation between non-lagged and lagged inputs. The function  $\text{corr}(f_s)$  is shown in the graph at the bottom of Fig. 6. The DSI and OSI are averaged over the  $32 \times 32$  cortical cells of one simulation run.

The mean DSI reaches a maximum of about 0.25 near  $f_s \approx 9.2$  Hz, which corresponds to  $\text{corr} = 0$ . At the same value for  $f_s$ , the mean OSI is at a minimum. The dashed line shows the OSI of the lagged inputs alone for comparison. If the correlation increases or decreases, the DSI decreases to zero and the OSI approaches the value of the non-lagged inputs. Both effects are due to an increasing positive or negative overlap  $m(x)$  between the lagged and the non-lagged spatial receptive fields. The overlap is defined as a number between  $-1$  and  $1$ ,

<sup>1</sup> Since the response function is real, the Fourier transform is always symmetric with respect to the origin

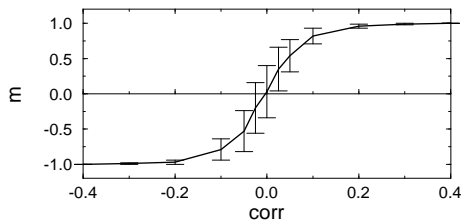


**Fig. 7.** The mean overlap as defined in (6), averaged over all  $32 \times 32$  cortical cells of one simulation run, has been plotted as a function of the temporal correlation  $\text{corr}$ . It can be recognized from the above figure that a small overlap can be obtained for weak correlations between non-lagged and lagged inputs. Only a small overlap  $m$ , however, is compatible with a spatial phase shift between non-lagged and lagged inputs, which in turn is necessary for the emergence of direction selectivity

$$m(\mathbf{x}) = \frac{\sum_{\alpha} J^{\text{D,nl}}(\mathbf{x}, \alpha) J^{\text{D,l}}(\mathbf{x}, \alpha)}{\sqrt{\left[ \sum_{\alpha} (J^{\text{D,nl}}(\mathbf{x}, \alpha))^2 \right] \left[ \sum_{\alpha} (J^{\text{D,l}}(\mathbf{x}, \alpha))^2 \right]}} \quad (6)$$

with  $J^{\text{D},\tau}(\mathbf{x}, \alpha) = J^{\text{ON},\tau}(\mathbf{x}, \alpha) - J^{\text{OFF},\tau}(\mathbf{x}, \alpha)$  for  $\tau \in \{\text{nl}, \text{l}\}$ . The mean  $m(\mathbf{x})$  averaged over all cortical neurons of one simulation run and its standard deviation have been plotted as a function of  $\text{corr}$  in Fig. 7. The overlap is very weak for correlations near zero and approaches the maximum and minimum value of  $\pm 1$  for  $\text{corr}(f_s) > 0.2$  and  $\text{corr}(f_s) < -0.2$ .

The growing or falling overlap has two effects, namely, a loss of the (random) spatial phase difference between non-lagged and lagged inputs resulting in a decreasing DSI, and an increasing alignment of the preferred orientations of the lagged and the non-lagged inputs leading to an increase of the total orientation selectivity index (OSI).

### 3.2 Variable correlations between non-lagged and lagged inputs

Throughout the previous subsection, we have assumed that the functional form of non-lagged or lagged inputs is the same for all such inputs. We now turn to a second scenario in which the above assumption is not made. In this scenario, the lagged response function and hence the correlation between non-lagged and lagged inputs depends in a random way on position  $\alpha$  in the LGN grid. We address the question whether and, if so, to what degree the simulation results we have described in Sect. 3.1 are stable against random fluctuations in the temporal part of the correlation function. To this end, the parameter  $f_s$  of the lagged input function is drawn from an interval according to a uniform distribution.

For the simulation runs summarized in Fig. 8, the interval of the  $f_s$  values is chosen in such a way that the mean temporal correlation is zero and the standard deviation of the correlation takes a certain assigned value. Both the mean direction selectivity index and the mean orientation selectivity index remain basically unchanged as the standard deviation is increased. In the last row of Fig. 8, the interval of the  $f_s$  values (solid bar) and the minimum and maximum values of the correlation (dashed bar) that correspond to a certain standard deviation are shown. Even when the correlation varied between  $-0.65$  and  $0.37$ , the mean direction selectivity index did not change significantly. If the mean correlation is

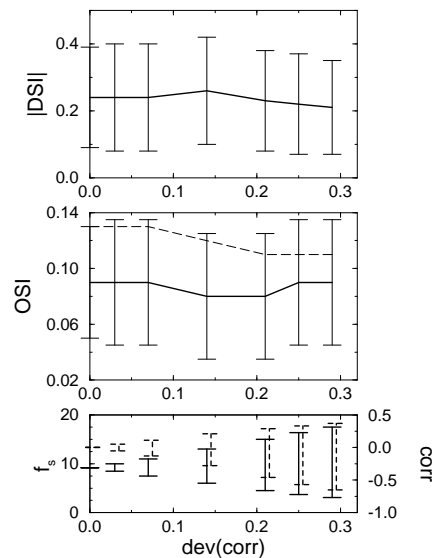


**Fig. 8.** The absolute values of the mean direction selectivity index (DSI) and the mean orientation selectivity index (OSI) have been plotted for the case of variable correlations between non-lagged and lagged inputs. For each LGN position  $\alpha$ , the  $f_s$  value is drawn from an interval that is indicated by the solid error bar in the bottom graph. The corresponding minimum and maximum values of  $\text{corr}$  are visualized by the dashed error bars. The interval is chosen in such a way that  $\langle \text{corr} \rangle = 0$ . Increasing the interval is equivalent to increasing the standard deviation  $\text{dev}(\text{corr})$  of the temporal correlation. The OSI of lagged inputs alone is plotted as a *dashed line* in the center graph for comparison

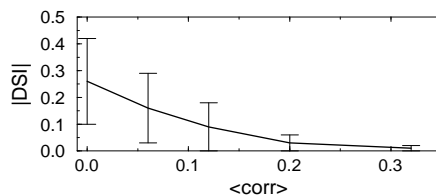


**Fig. 9.** The dependence of the direction selectivity index (DSI) upon the mean correlation  $\langle \text{corr} \rangle$  between non-lagged and lagged inputs is displayed for scenario II. The parameter  $f_s$  is drawn from such an interval that a certain assigned value of  $\langle \text{corr} \rangle$  and a standard deviation of  $\text{dev}(\text{corr}) = 0.14$  are obtained. The angular brackets denote an average for all  $23 \times 23$  cells of one simulation run

increased and the standard deviation is kept fixed, the direction selectivity index drops in the same way as in the case of constant correlations; cf. Fig. 9 and Fig. 6.

To summarize, to obtain strongly direction-selective receptive fields not *all* inputs have to be tuned in such a way that the temporal correlation between lagged and non-lagged inputs is as low as in Sect. 3.1. A necessary requirement, however, is, that the *mean* temporal correlation assumes a low value.

At the moment there is no experimental evidence for the validity of the requirement that the mean temporal correlation between non-lagged and lagged inputs be low. We can only give arguments for its plausibility based on a model of linear response; cf. [27], Sect. 3. First, if one chooses parameter values for the linear response function of the non-lagged and lagged inputs that are in agreement with measurements of Saul and Humphrey [22], the resulting  $\text{corr}$  is small. Second, from an information processing point of view, it seems

reasonable to use orthogonal functions to analyze different aspects of the inputs. Orthogonality of the two linear response functions, however, is equivalent to a vanishing temporal correlation function  $\text{corr}$ .

### 3.3 Direction selectivity due to intracortical interaction

In both scenarios considered so far, direction selectivity is due to a spatiotemporally non-separable distribution of the weights from the LGN to the cortex. In the following we investigate a variant of the scenario described in Sect. 3.1, in which positive or negative correlations between the two types of temporal input no longer allow a (nearly) independent development of non-lagged and lagged synapses. Instead, the overlap (6) between the non-lagged and lagged weights approaches  $m = \pm 1$ , as is illustrated by Fig. 7. Within these limits, the spatiotemporal receptive fields can be written

$$Q(\mathbf{x}, \boldsymbol{\alpha}, t) = Q(\mathbf{x}, \boldsymbol{\alpha})[L^{\text{nl}}(t) \pm L^{\text{l}}(t)], \quad (7)$$

with  $Q(\mathbf{x}, \boldsymbol{\alpha}) = J^{\text{ON,nl}}(\mathbf{x}, \boldsymbol{\alpha}) - J^{\text{OFF,nl}}(\mathbf{x}, \boldsymbol{\alpha})$ . Since the receptive field is spatiotemporally separable, direction selectivity is lost.

We will now propose a simple cortical wiring scheme that gives rise to direction-selective receptive fields, even if the weight distribution from the LGN to the cortex is spatiotemporally separable. To this end we consider two groups, A and B, of cortical neurons that each form a cortical orientation map. A schematic drawing of our model can be found in Fig. 10. Neurons in the two groups are assumed to receive ON and OFF inputs with a non-lagged and a lagged temporal response characteristic from the LGN. However, cortical cells in the two groups are linked to different layers in the LGN, which can result in a different time structure for non-lagged and lagged inputs and, furthermore, in a different sign of the temporal correlation  $\text{corr}$  for the two groups.

During development there is no coupling between the two groups, so that two uncorrelated maps  $Q^A(\mathbf{x}, \boldsymbol{\alpha})$  and  $Q^B(\mathbf{x}, \boldsymbol{\alpha})$  develop. We now turn to the emerging temporal response structure. We assume that  $\text{corr} > 0.2$  for group A and  $\text{corr} < -0.2$  for group B. This results in an overlap  $m = 1$  and  $Q^A(\mathbf{x}, \boldsymbol{\alpha}, t) = Q^A(\mathbf{x}, \boldsymbol{\alpha})[L^{\text{nl}}(t) + L^{\text{l}}(t)]$  for group A, whereas  $m = -1$  and  $Q^B(\mathbf{x}, \boldsymbol{\alpha}, t) = Q^B(\mathbf{x}, \boldsymbol{\alpha})[L^{\text{nl}}(t) - L^{\text{l}}(t)]$  is obtained for group B. The receptive fields for the two groups are spatiotemporally separable and, hence, not direction selective. Both the spatial and the temporal part of the receptive field are, however, different for the two groups.

After the receptive field structure for the two maps has been established, further intracortical connections in addition to the ones between neighboring neurons within one cortical map develop. These connections link neurons of the two groups whose receptive fields cover the same area in the visual field. These types of connection are common among cortical maps [19]. The effect of these intracortical connections is modeled by summing the outputs of the linked cells. A combined spatiotemporal receptive field then takes the form

$$Q(\mathbf{x}, \boldsymbol{\alpha}, t) = Q^A(\mathbf{x}, \boldsymbol{\alpha})[L^{\text{nl}}(t) + L^{\text{l}}(t)] + Q^B(\mathbf{x}, \boldsymbol{\alpha})[L^{\text{nl}}(t) - L^{\text{l}}(t)]. \quad (8)$$

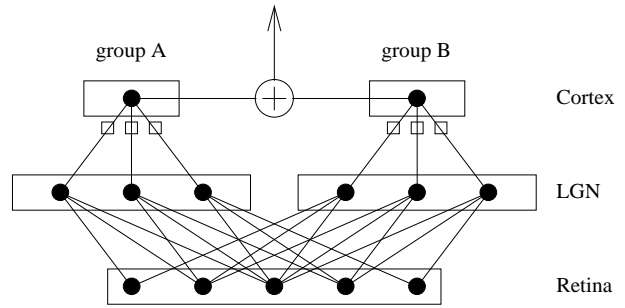


**Fig. 10.** Connectivity of the third scenario. Two cortical neurons from group A and B and their underlying visual pathway are displayed schematically. The receptive fields of both neurons cover the same area in the visual field. They are therefore fed by the same photoreceptors in the retina. However, cortical neurons from group A and B receive inputs from different layers of the LGN, as indicated by the separate rectangles. Intracortical processing between the two groups has been modeled in an extremely simplified way, i.e., by simply adding the outputs of the two neurons

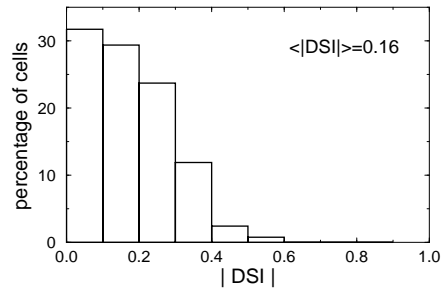


**Fig. 11.** Distribution of the absolute value of the direction selectivity index for the third scenario. Neurons in group A received lagged input with  $f_s = 15.3$  Hz, neurons in group B with  $f_s = 5.8$  Hz. Therefore, non-lagged and lagged inputs are positively correlated for group A [ $\text{corr}(15.3) = 0.3$ ] and negatively correlated for group B [ $\text{corr}(5.8) = -0.3$ ]

These receptive fields are no longer spatiotemporally separable and may show direction selectivity.

The mechanism that underlies direction selectivity in this scenario is quite similar to the one described in Sect. 3.1; cf. Fig. 1. Two separable receptive fields that differ in their spatial phase (and orientation) in a random way and that have different temporal response functions are added. The upshot is that combined receptive fields with a varying degree of direction selectivity emerge. Figure 1 applies to the third scenario as well, if  $L^{\text{nl}}(t)$  is replaced by  $L^{\text{nl}}(t) + L^{\text{l}}(t)$  and  $L^{\text{l}}(t)$  by  $L^{\text{nl}}(t) - L^{\text{l}}(t)$ . The distribution of the DSI has been plotted in Fig. 11 for a simulation run with  $f_s = 15.3$  Hz for the layer in the LGN that projects to cells in group A, and  $f_s = 5.8$  Hz for the layer that projects to cells in group B. These values of  $f_s$  correspond to temporal correlations of  $\text{corr}(15.3) = 0.3$  and  $\text{corr}(5.8) = -0.3$ . The distribution is in agreement with results from reverse correlation measurements; cf. Fig 17.a in [3].

We will briefly mention two possible variants of this scenario. First, one could assume that non-lagged and lagged inputs grow into different cortical sub-layers and form two cortical maps of their own. If these two cortical maps develop independently initially, and if subsequently intracortical connections grow between those cells whose receptive fields correspond to the same retinotopic position, direction-selective receptive fields emerge in the same way as de-

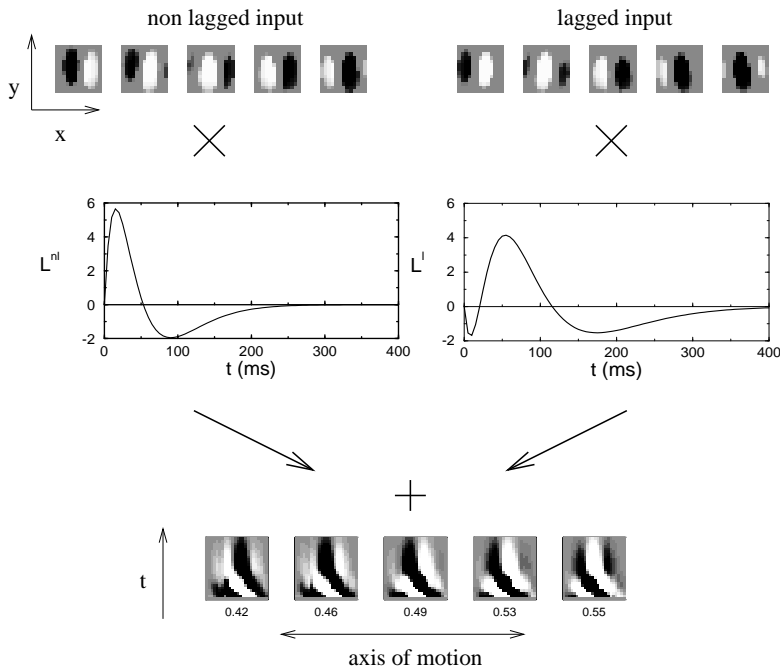


**Fig. 12.** The receptive fields of five neighboring cells of the whole  $32 \times 32$  grid are shown for the case of a narrow bar of light sweeping across the retina from left to right at a speed of  $v = 15^\circ/s$ . This corresponds to the correlation functions shown in [27], Fig. 4. The subplots are arranged in the same way as in Fig. 1. All receptive fields are oriented along the  $y$ -axis and respond strongly to rightward motion. As has been discussed in Sect. 3.1 (cf. also Fig. 5), a spatial phase shift between non-lagged and lagged inputs that can be clearly recognized in the first line of the above figure underlies the emergence of direction-selective receptive fields

scribed above. The only difference is that, in formula (8), the expression  $L^{nl}(t) + L^l(t)$  has to be replaced by  $L^{nl}(t)$  and  $L^{nl}(t) - L^l(t)$  by  $L^l(t)$ . Consistent with this, simple cells with exclusively lagged-like temporal responses are found in the lower part of layer 4 (and the adjacent upper layer 5) in cat V1 [23], suggesting that these cells receive exclusively lagged-cell LGN input. However, the orientation maps of these simple cells may well be linked to that of the cells in adjacent sub-layers receiving non-lagged input.

Second, the development of the intracortical connections could also follow some type of Hebbian rule. Then cells with correlated outputs would be linked automatically. If oriented waves that sweep across the retina [17] or LGN [11, 16] drive the development during this period, rather than uncorrelated noise, this would lead to linkage of two receptive fields that cover the same area in the visual field and respond to similar preferred orientations, but that may differ in spatial phase. We will describe simulation results for this case in a future article.

### 3.4 Development in an environment of moving gratings

Throughout the first three scenarios, the development of spatiotemporal receptive fields was driven by uncorrelated noise in the photoreceptors. In contrast, we now turn to the case of structured input during the growth of the synapses. There are various sources of structured input to the photoreceptors, including spontaneous activity waves during sleep [11, 16] and natural visual input.

In [27], Sect. 3, we have derived the correlation functions for the case of narrow bars moving across the retina in one particular direction; cf. Fig. 4 in [27]. As a first step, we will now investigate the development under this special type of correlation function. As a second step, we will then turn to the more general case of patterns that move in arbitrary directions across the retina.

The outcome of a typical simulation for the case of a narrow bar of light moving from left to right is shown in Fig. 12. The corresponding correlation function is displayed in [27], Fig. 4. The subplots in Fig. 12 are arranged in the same way as the subplots in Fig. 1. In the top line of Fig. 12, the differences between the synaptic weights of ON and OFF inputs are displayed for a  $1 \times 5$  detail of the whole  $32 \times 32$  grid, separately for non-lagged and lagged inputs. To obtain the spatiotemporal receptive fields shown in the bottom line of Fig. 12, the non-lagged and lagged inputs are multiplied by their corresponding temporal response functions, added, and subsequently integrated along their preferred orientation. As becomes obvious from the subplots for non-lagged and lagged inputs, all receptive fields are oriented perpendicularly to the direction of motion. Furthermore, all lagged inputs show a spatial shift to the left as compared to the non-lagged inputs. This results in a strong direction selectivity of the spatiotemporal receptive fields for leftward motion, as can be recognized from the high positive direction selectivity index noted under the spatiotemporal receptive fields in Fig. 12. The direction selectivity is due to a spatial phase shift between non-lagged and lagged inputs, as has been discussed in detail in Sect. 3.1.

It can be understood easily why receptive fields with a spatial phase shift between non-lagged and lagged inputs develop in a model of correlation based learning, if moving patterns are presented as an input to the retina. A synapse will grow if the input fed into this synapse is correlated to all other inputs. For the case of patterns moving from left to right, a strong correlation between non-lagged and lagged inputs corresponds to a spatial shift of the lagged inputs to the left as compared to the non-lagged inputs, since the spatial shift compensates for the delayed response of the lagged inputs.

We now turn to the general case of patterns sweeping across the retina with varying directions of motion. To model

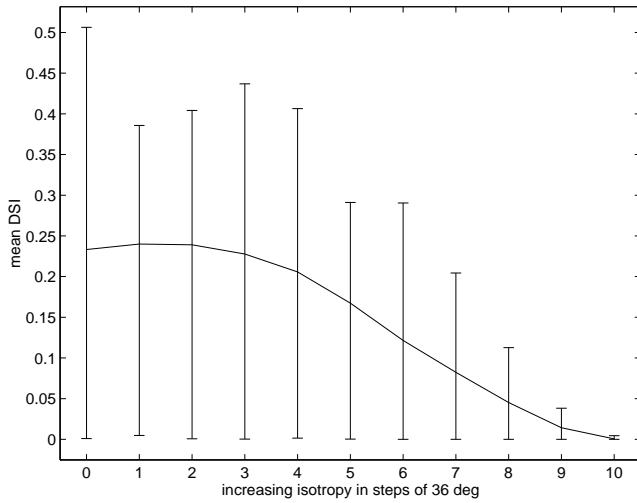


**Fig. 13.** The mean direction selectivity index (DSI) has been plotted against the range of directions of motion that were present during development. This situation has been modeled by averaging the correlation function for this case over the corresponding range of angles; cf. Fig. 4 in [27]. The error bars indicate the maximum and minimum values obtained during a simulation run. As the isotropy of the correlation function increases, the direction selectivity is lost

this situation, the correlation function in [27], Fig. 4, is averaged over different directions, resulting in rotationally symmetric correlation functions. In Fig. 13, the mean direction selectivity index has been plotted against the range of directional angles for which the average was calculated.

It becomes obvious that, as the range of angles and hence the isotropy of the correlation function increases, the direction selectivity of the receptive fields vanishes. This is due to a loss of the spatial phase shift between non-lagged and lagged inputs.

Similar results are obtained if the correlation function of Fig. 4 in [27] is rotated during a simulation run. Direction-selective receptive fields will develop only if the rotation is not performed too quickly. In this case, however, the distribution of the directions of motion the cells are sensitive to will not be isotropic, as is illustrated by the following example. In Fig. 14 a direction selectivity map on a  $32 \times 32$  grid of neurons has been plotted for the case where the correlation function is rotated by a multiple of  $90^\circ$  at every eighth timestep. The whole simulation run took 22 timesteps. The small lines indicate the preferred orientation of a cell, whereas the arrows indicate the preferred direction of motion. The degree of direction selectivity corresponds to the length of the arrow. Cells with different degrees of direction selectivity emerge from the development. The mean direction selectivity index takes a value of 0.15.

In Fig. 15 the preferred orientations of non-lagged and lagged inputs are displayed separately. The preferred orientations of non-lagged and lagged inputs are well aligned and, hence, do not rotate in time as may happen in the first three scenarios. However, as was noted above and as can be recognized in Fig. 14, the cells develop a weak preference for downward motion on average, due to the comparatively slow rotation of the correlation function. If one reduces the number of timesteps during which a particular direction of motion is presented, the preferred directions of motion of

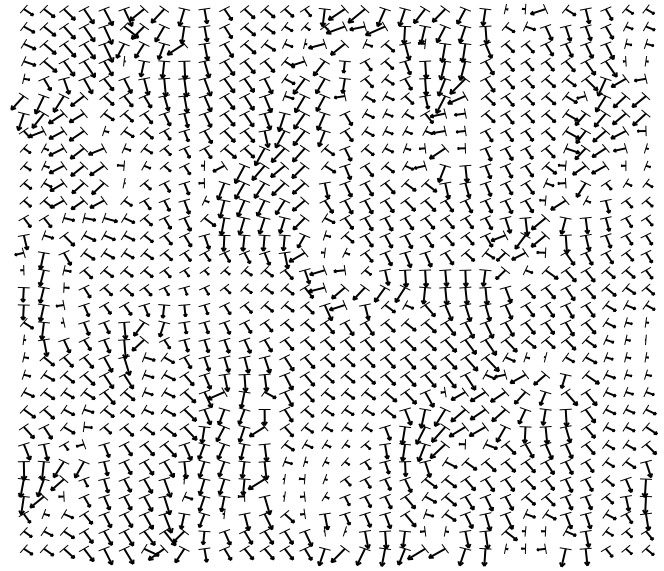


**Fig. 14.** Direction selectivity map for the case of structured input with patterns moving across the retina in arbitrary directions of motion. We model this situation by rotating the correlation function in [27], Fig. 4 at every eighth timestep during a simulation run. For every cell of the whole  $32 \times 32$  grid, the preferred direction of motion is coded by a small arrow whose length corresponds to the degree of direction selectivity. The lines perpendicular to the arrows symbolize the preferred orientation of the cells. Different cells show a preference for different directions of motion with widely varying degrees of direction selectivity

different cells become distributed more isotropically, but at the expense of a decreasing mean direction selectivity.

We conclude that in an environment of moving gratings and for a linear Hebbian rule, as is used in this article, direction selective receptive fields develop only if the correlation function that drives the development is not completely isotropic. A possible nonlinear extension of our Hebbian rule that can result in direction-selective receptive fields even for the isotropic case has been proposed recently by Feidler et al. [7].

#### 4 Results: analysis

Let us start by considering the case where lagged and non-lagged inputs have identical preferred orientations. Then, as shown previously (Sect. 3.3; Eq. 7), either a  $0^\circ$  or a  $180^\circ$  spatial phase difference between lagged and non-lagged inputs leads to a spatiotemporally separable receptive field. Thus, an intermediate spatial phase difference is a prerequisite for direction selectivity of the linear spatiotemporal receptive field. Intuitively, direction-selective receptive fields result when lagged and non-lagged inputs are approximately in quadrature, i.e. about  $90^\circ$  apart in spatial phase.

For such a receptive field to result from a correlation-based rule, the non-lagged inputs of a given center-type at a given spatial position  $\alpha$  are to be “best-correlated” with lagged inputs of the same center-type at some shifted spatial position  $\alpha - \epsilon$ , where  $\epsilon$  points in the preferred direction. Such correlations will exist, if the lagged inputs at  $\alpha - \epsilon$  tend to receive excitation somewhat before the non-lagged inputs at  $\alpha$ , with a time delay corresponding to the differ-

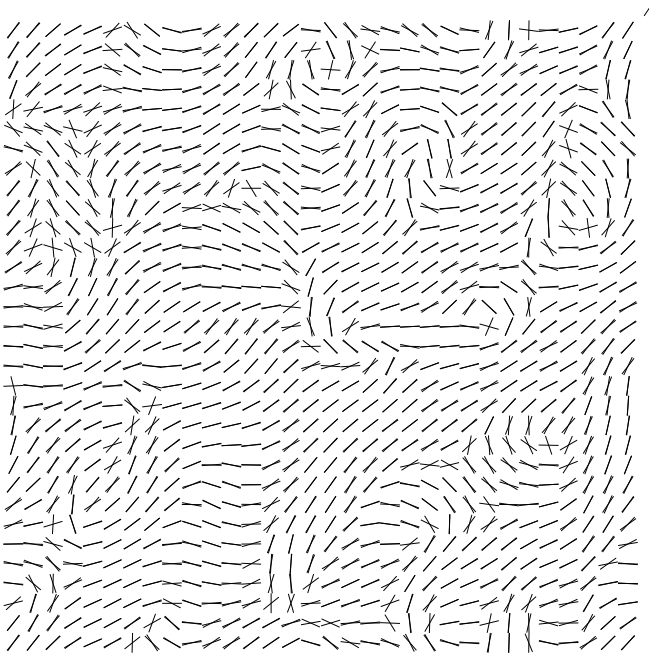


**Fig. 15.** The preferred orientations for non-lagged and lagged inputs are displayed separately for the simulation run of Fig. 14. In contrast to the first three scenarios, both orientations are well aligned, that is, the preferred orientation does not change with time

ence between lagged and non-lagged response times. This occurs naturally in an environment of gratings drifting at an appropriate velocity in the direction  $\epsilon$ . However, a grating moving in the opposite direction with the same velocity will best correlate the same non-lagged cells at  $\alpha$  with a set of lagged cells at  $\alpha + \epsilon$ , that is, shifted in the opposite spatial direction. Assuming that the functional form of the lagged response is independent of the LGN position  $\alpha$ , then averaging over gratings moving in both directions will lead the non-lagged/lagged correlations to be symmetric about spatial separation 0. This is sufficient to prevent the development of spatial phase shifts other than  $0^\circ$  or  $180^\circ$  if preferred orientations are matched, as we will show below.

This is the intuitive reason why we can only achieve direction selectivity in our model by (a) decorrelating lagged and non-lagged inputs so that their developments are independent and their preferred orientations are not matched or (b) allowing weights to develop in an anisotropic environment, or at least one that is anisotropic when averaged over a time relevant to receptive field development. If preferred orientations are matched and correlations are symmetric about spatial separation 0, direction selectivity will not arise from our simple linear rule.

We now show why a symmetric correlation function prevents development of direction selectivity, if lagged and non-lagged preferred orientations are matched. For the scenarios described in Sects. 3.1 and 3.3 the functional form of the lagged response is independent of the LGN position  $\alpha$ , and the correlation function factorizes into a spatial and a temporal part:  $C^{c,c';\tau,\tau'}(\alpha, \alpha') = C^{\tau,\tau'} C^{c,c'}(\alpha, \alpha')$  for  $c = \text{ON,OFF}$  and  $\tau = \text{nl,l}$ , with  $C^{\tau,\tau'}$  given by Eq. (19) in [27]. Note that  $C^{\tau,\tau'} = C^{\tau',\tau}$ . The spatial correlations should obey  $C^{c,c'}(\alpha, \alpha') = C^{c',c}(\alpha', \alpha)$ , that is, the corre-

lation of the activities of two inputs does not depend on the order in which the two are considered. By translation invariance, these correlations depend only on the spatial separation of two inputs, and not on each position separately:  $C^{c,c'}(\alpha, \alpha') = C^{c,c'}(\alpha - \alpha')$ . If the spatial correlation functions are also symmetric about zero,  $C^{c,c'}(\mathbf{x}) = C^{c,c'}(-\mathbf{x})$ , then the correlation functions are unchanged under interchange of  $c$  and  $c'$ :  $C^{c,c'}(\mathbf{x}) = C^{c',c}(\mathbf{x})$ .

With these assumptions, the developmental equation (1) is unchanged when  $\tau$  and  $\tau'$  interchange and also when  $c$  and  $c'$  interchange. As analyzed in [6, 20] and by Erwin and Miller (unpublished manuscript), because of these two symmetries, (1) may be diagonalized by transformation to the following basis,

$$J^{SS} = (J^{\text{ON,l}} + J^{\text{OFF,l}}) + (J^{\text{ON,nl}} + J^{\text{OFF,nl}}), \quad (9)$$

$$J^{SD} = (J^{\text{ON,l}} + J^{\text{OFF,l}}) - (J^{\text{ON,nl}} + J^{\text{OFF,nl}}), \quad (10)$$

$$J^{DS} = (J^{\text{ON,l}} - J^{\text{OFF,l}}) + (J^{\text{ON,nl}} - J^{\text{OFF,nl}}), \quad (11)$$

$$J^{DD} = (J^{\text{ON,l}} - J^{\text{OFF,l}}) - (J^{\text{ON,nl}} - J^{\text{OFF,nl}}). \quad (12)$$

Here, ‘S’ stands for sum and ‘D’ for difference; the first superscript in  $J^{AB}$ ,  $A, B \in \{S, D\}$ , tells whether center types are summed or subtracted, and the second superscript tells the same for temporal types. The linear developments (before synaptic saturation is reached, Eq. 3) of  $J^{SS}$ ,  $J^{SD}$ ,  $J^{DS}$ , and  $J^{DD}$  are independent of one another. Their unconstrained developments are determined by:

$$\begin{aligned} \frac{dJ^{AB}(\mathbf{x}, \alpha, t)}{dt} &= \lambda A(\mathbf{x} - \alpha) \sum_{\mathbf{x}'} I(\mathbf{x}, \mathbf{x}') \\ &\times \sum_{\alpha'} C^{AB}(\alpha, \alpha') J^{AB}(\mathbf{x}', \alpha', t) \end{aligned} \quad (13)$$

where, using  $C^{l,l} = C^{\text{nl,nl}} = 1$  and  $C^{l,nl} = C^{\text{nl,l}} = \text{corr}$  (cf. Eq. 20 in [27]),<sup>2</sup>

$$C^{SS} = (C^{\text{ON,ON}} + C^{\text{ON,OFF}})(1 + \text{corr}), \quad (14)$$

$$C^{SD} = (C^{\text{ON,ON}} + C^{\text{ON,OFF}})(1 - \text{corr}), \quad (15)$$

$$C^{DS} = (C^{\text{ON,ON}} - C^{\text{ON,OFF}})(1 + \text{corr}), \quad (16)$$

$$C^{DD} = (C^{\text{ON,ON}} - C^{\text{ON,OFF}})(1 - \text{corr}). \quad (17)$$

The constraints (2) alter only the equation for  $J^{SS}$ , subtracting  $4\epsilon(\mathbf{x})A(\mathbf{x} - \alpha)$  from that equation in (13).

Let  $e_i^{\text{AB}}(\mathbf{x}, \alpha)$  be the  $i^{\text{th}}$  eigenfunction of the linear development equation for  $J^{\text{AB}}$ , with eigenvalue  $\lambda_i^{\text{AB}}$ , and let  $J_i^{\text{AB}}(0)$  be the component of this eigenvector in the initial ( $t = 0$ ) random weight configuration. Then the solutions to the linear developmental equations can be written

$$J^{\text{AB}}(\mathbf{x}, \alpha, t) = \sum_i J_i^{\text{AB}}(0) \exp(\lambda_i^{\text{AB}} t) e_i^{\text{AB}}(\mathbf{x}, \alpha). \quad (18)$$

The eigenfunctions corresponding to the largest eigenvalues will grow fastest and reach the upper and lower bounds first, where the weights are frozen. The structure of the emergent receptive fields will therefore resemble closely the leading eigenfunctions of the development equation, that is, they should approximate a mixture of the  $e_i^{\text{AB}}(\mathbf{x}, \alpha)$  with the largest eigenvalues  $\lambda_i^{\text{AB}}$ .

<sup>2</sup> Note, by the assumed symmetries, that  $C^{\text{ON,ON}} = C^{\text{OFF,OFF}}$ ,  $C^{\text{ON,OFF}} = C^{\text{OFF,ON}}$

The patterns  $J^{\text{DS}}$  and  $J^{\text{DD}}$  are of particular interest since they describe the difference between ON and OFF inputs. Furthermore, these patterns are expected to have the largest eigenvalues. Because the linear constraints exclusively affect the development of  $J^{\text{SS}}$ , and lower its eigenvalues, these leading eigenfunctions are not expected to include patterns of  $J^{\text{SS}}$ . Finally, on the assumption that  $C^{\text{ON,OFF}}$  is roughly of opposite sign as a function of distance to  $C^{\text{ON,ON}}$  (e.g. [14, 15, 17]),  $(C^{\text{ON,ON}} - C^{\text{ON,OFF}})$  will generate larger eigenvalues than  $(C^{\text{ON,ON}} + C^{\text{ON,OFF}})$ . Thus, we assume that the leading eigenfunctions will be those of  $J^{\text{DS}}$  and/or  $J^{\text{DD}}$ , and restrict attention to those two weight structures.

We consider three cases:  $\text{corr} \approx 1$ ,  $\text{corr} \approx -1$ , and  $\text{corr} = 0$ .

1. For  $\text{corr} \approx 1$ ,  $J^{\text{DS}}$  dominates. Growth of a spatial pattern  $e_i^{\text{DS}}(\mathbf{x}, \boldsymbol{\alpha})$  of  $J^{\text{DS}}$  represents growth of a pattern proportional to  $J^{\text{ON,l}}(\mathbf{x}, \boldsymbol{\alpha}) = J^{\text{OFF,nl}}(\mathbf{x}, \boldsymbol{\alpha}) = e_i^{\text{DS}}(\mathbf{x}, \boldsymbol{\alpha})$ ,  $J^{\text{OFF,l}}(\mathbf{x}, \boldsymbol{\alpha}) = J^{\text{ON,nl}}(\mathbf{x}, \boldsymbol{\alpha}) = -e_i^{\text{DS}}(\mathbf{x}, \boldsymbol{\alpha})$ . That is, development of  $J^{\text{DS}}$  corresponds to identical receptive fields for lagged and non-lagged inputs: identical preferred orientations and  $0^\circ$  spatial phase difference.
2. For  $\text{corr} \approx -1$ ,  $J^{\text{DD}}$  dominates. Growth of a spatial pattern  $e_i^{\text{DD}}(\mathbf{x}, \boldsymbol{\alpha})$  of  $J^{\text{DD}}$  represents growth of a pattern proportional to  $J^{\text{ON,l}}(\mathbf{x}, \boldsymbol{\alpha}) = J^{\text{OFF,nl}}(\mathbf{x}, \boldsymbol{\alpha}) = e_i^{\text{DD}}(\mathbf{x}, \boldsymbol{\alpha})$ ,  $J^{\text{OFF,l}}(\mathbf{x}, \boldsymbol{\alpha}) = J^{\text{ON,nl}}(\mathbf{x}, \boldsymbol{\alpha}) = -e_i^{\text{DD}}(\mathbf{x}, \boldsymbol{\alpha})$ . That is, development of  $J^{\text{DD}}$  corresponds to opposite receptive fields for lagged and non-lagged inputs: identical preferred orientations and  $180^\circ$  spatial phase difference.
3. For  $\text{corr} = 0$ ,  $J^{\text{DS}}$  and  $J^{\text{DD}}$  are determined by the same linear operator, and thus have identical eigenvectors and eigenvalues. Because of this degeneracy, the development can equally be described as independent development of any two orthogonal linear combinations of  $J^{\text{DS}}$  and  $J^{\text{DD}}$ . In particular, we can choose  $(J^{\text{DS}} + J^{\text{DD}})/2 = (J^{\text{ON,l}} - J^{\text{OFF,l}})$  and  $(J^{\text{DS}} - J^{\text{DD}})/2 = (J^{\text{ON,nl}} - J^{\text{OFF,nl}})$ . Thus, lagged and non-lagged receptive fields develop independently: preferred orientations of lagged and non-lagged inputs are in general not matched.

Thus, for  $\text{corr}$  sufficiently large in absolute value, lagged and non-lagged inputs develop with identical preferred orientations and with spatial phase shifts of either  $0^\circ$  or  $180^\circ$ . For  $\text{corr}$  sufficiently small in absolute value, lagged and non-lagged inputs develop independently, and preferred orientations are not matched. The only remaining question is what will happen for intermediate values of  $\text{corr}$ , and the answer is shown in Fig. 7: for  $|\text{corr}| \geq 0.2$ , receptive fields are essentially identical to the case  $|\text{corr}| = 1$ : perfect overlap ( $\text{corr} > 0$ ) or perfect anti-overlap ( $\text{corr} < 0$ ). As  $\text{corr}$  decreases below about 0.2, there is a gradual unlinking of lagged and non-lagged maps, and orientations gradually become independent as direction selectivity gradually emerges.<sup>3</sup>

In the fourth scenario described in Sect. 3.4 the correlation function does not factorize into a spatial and a temporal part. However, if patterns with all directions of motion sweep across the retina during development, the correlation function for this scenario (see Fig. 4 in [27]) has to be averaged

<sup>3</sup> This result (expressed in terms of eigenvalues in a form that, for the present model, becomes  $|(1 + \text{corr}) - (1 - \text{corr})| \leq 1/3(1 + |\text{corr}|)$ , which is equivalent to  $|\text{corr}| \leq 0.2$ ), was first obtained in the context of a different model in [6]

over arbitrary directions and becomes isotropic. In this case the correlation function depends only on the spatial separation and remains unchanged when  $\tau$  and  $\tau'$  and also  $c$  and  $c'$  interchange. Therefore, the developmental equations can be transformed to the basis (9) to (12), as well. Using similar arguments as above one can show that either  $J^{\text{DS}}$  or  $J^{\text{DD}}$  dominates the dynamics. Hence, if the eigenvalues corresponding to  $J^{\text{DS}}$  and  $J^{\text{DD}}$  are not degenerate, receptive fields for lagged and non-lagged inputs with identical preferred orientations and either  $0^\circ$  or  $180^\circ$  spatial phase difference will emerge, while if they are degenerate, lagged and non-lagged receptive fields will be uncorrelated.

In summary, direction selectivity cannot develop from the simple linear model studied here unless (a) lagged and non-lagged inputs develop independently, leading to non-matching of preferred orientations, or (b) correlation functions are anisotropic, and in particular are asymmetric about zero.

## 5 Discussion

We have proposed a developmental model for the origins of direction selectivity of simple cells. In our model, direction selectivity is based on the convergence of four types of spatiotemporal input channels onto a simple cell, that is, non-lagged ON and OFF channels and lagged ON and OFF channels. These input channels are described by linear spatial and temporal response functions.

Extending an earlier and purely spatial model of Miller [18] to the spatiotemporal case, the development of spatiotemporal receptive fields is described as a Hebbian learning process. The essential quantities that determine the outcome of the development are spatial and temporal correlations between different input channels. We have discussed four different scenarios. The first three scenarios cover the development before eye-opening. At this time, direction-selective receptive fields can already be observed experimentally [9]. We assume that the development during this period is driven by uncorrelated noise in the photoreceptors. For the case of a weak *mean* correlation between non-lagged and lagged channels, the maps of the two types of temporal input develop nearly independently. If one separately considers the spatial receptive fields of non-lagged and lagged inputs that converge onto one cortical cell, one will notice that these two receptive fields may have a different orientation and a difference in spatial phase. A difference in phase is responsible for the emergence of spatiotemporally *non-separable* and hence direction-selective receptive fields, whereas a difference in the preferred orientation of non-lagged and lagged inputs corresponds to a rotation of the preferred orientation in time. Receptive fields with preferred orientation that drifts in time seem to be uncommon [2, 3, 26], at least in adult animals, although there are some reports of such cells [21, 24]. A developmental mechanism that results in this type of receptive field, however, could underlie the earliest development of direction selectivity, after which receptive fields could be modified by vision. This could be tested by studying the temporal invariance of preferred orientation in young animals. In the third scenario, direction selectivity is due to a simple intracortical inter-

action between two cortical maps that differ in their temporal response characteristic. Again, preferred orientations will tend to rotate in time. If one compares the outcome of a simulation of our model with experimental data, it turns out that both in our model and in reverse correlation studies [3], cells with widely varying degrees of direction selectivity can be observed, and the distribution of the direction selectivity index for a population of cells matches well the distribution obtained from reverse correlation measurements.

As a simple model for the development after eye-opening, we have studied in the fourth scenario the emergence of spatio-temporal receptive fields in an environment of moving lines or gratings. If patterns with only one particular direction of motion are presented, the cells will develop a selectivity for this particular direction. If multiple directions of motion are present but receptive fields are determined over periods in which only a subset of directions is seen, again direction selectivity can emerge. In these scenarios, direction selectivity develops with matched preferred orientations for lagged and non-lagged inputs to a cell, and thus without a prediction that preferred orientations should rotate in time. This is achieved at the cost of assuming that receptive fields become determined over times in which only a subset of directions of motion are seen, and as a result it is difficult to avoid having a bias among the ensemble of cortical cells for a particular subset of preferred directions. As the distribution of the directions of motion present during receptive field development becomes more and more isotropic, direction selectivity is gradually lost.

Concurrently with the present work, Feidler et al. [7] suggested that inclusion of simple, biological non-linearities in postsynaptic activation, so that plasticity is suppressed when the postsynaptic cell receives little input, can cause a breaking of symmetry: a receptive field can learn one or the other direction in an environment in which both directions are seen equally often. After averaging over input patterns, this would mean the following. Suppose a correlation function shows peaks at non-zero spatial separation that are symmetrically placed about separation 0. Then receptive fields would be able to converge to sets of lagged and non-lagged inputs separated by a distance corresponding to one or the other peak, rather than “averaging out the peaks” to produce  $0^\circ$  or  $180^\circ$  phase shifts as in the present model. This represents an interesting extension to the scenarios studied in this article, and clearly should be explored further. In particular, one would have to clarify whether direction selectivity will still emerge in an environment of patterns with a distribution of velocities that peaks at zero. In this case the correlation function assumes its maximum at spatial separation zero and it is unclear whether a symmetry breaking as described in [7] still takes place.

One of the main assumptions underlying our model is that an approximately equal number of lagged and non-lagged inputs from the LGN project onto a cortical simple cell. Saul and Humphrey report on about 40% lagged and 60% non-lagged LGN cells in the sample they recorded from [22]. Other groups found a much lower number of lagged LGN cells, which seems to be mainly due to different types of electrodes used by these groups as compared to those used by Saul and Humphrey (DeAngelis, Ohzawa and Alonso, personal communication, 1995).

In our model we have included intracortical interactions in a schematic way. First, synapses that link neighboring neurons of a single cortical map are modeled by a simple Mexican hat interaction that acts instantaneously and has the effect of coupling the receptive fields of neighboring cortical neurons during development. The structure of the spatiotemporal receptive field is assumed to be basically not affected by this interaction function. Second, intracortical interaction between *different* cortical maps has been captured in the scenario of Sect. 3.3 by simply adding corresponding receptive fields from the two maps. It has been demonstrated how such an interaction can result in a direction-selective response. It is well known, however, that intracortical interactions may have further important effects on the response properties of cortical cells, and we outline below some directions in which our model can be modified or extended to take a more realistic intracortical interaction into account.

It should be noted first that, by employing a model of linear response, we have implicitly assumed some sort of additional intracortical processing. This is due to the fact that the most plausible model to establish an approximately linear response of a simple cell is a pair of neurons that inhibit each other. The ON subregions of one of these neurons overlap with the OFF subregions of the other, and vice versa [8]. In our model such a pair of neurons can be considered as one entity. If both neurons cover the same input area, an exactly antagonistic pair of receptive fields would be learned because of the mutual inhibition of the two neurons, which would finally result in the approximately linear response of the cell.

Intracortical interactions could induce an additional directional bias in the spatiotemporal receptive field of the simple cell [29]. In particular, asymmetric intracortical inhibition combined with some sort of delay or low-pass filtering could implement a sort of Barlow-Levick motion detector [1], as in some recent models of simple cell direction selectivity [5, 13, 28]. As long as this type of interaction can be described by a linear response function, it is straightforward to implement the additional temporal structure in a model of spatiotemporal Hebbian learning.

Furthermore, some authors have proposed that excitatory feedback loops balanced by intracortical inhibition might be important to sharpen the receptive fields of simple cells and to explain observed degrees of orientation [25] and direction selectivity [5, 12]. We did not include these sorts of non-linearity in our model because our focus was on investigating the structure of spatiotemporal receptive fields and their development as revealed by reverse correlation measurements. The reverse correlation technique is an intrinsically linear approach.

In conclusion, we would like to stress again that our main intention was not to explain the exact response behavior of simple cells, but to demonstrate how the concept of correlation-based learning can be applied to the development of spatiotemporal receptive fields. In doing so, we have concentrated on the case where the convergence of non-lagged and lagged inputs onto a cortical cell provides the main source of temporal structure in the response of simple cells. Whether this is actually the case, or whether intracortical interaction is a primary source of receptive field

temporal structure, remains an open question requiring further experimental and theoretical studies for its resolution.

*Acknowledgements.* The authors thank E. Erwin for providing an elaborated version of a program of K.D.M. that was used for some of the simulations in this article, and for many useful discussions and suggestions. G.C. DeAngelis, J. Alonso, and M. Meister provided helpful information about their experimental work. Discussions with W. Gerstner are also greatly appreciated. S.W. acknowledges the hospitality of the Keck Center at UCSF, where part of this work was done. He was supported by a grant from the Studienstiftung des deutschen Volkes, which also made his stay at UCSF possible. K.D.M. is supported by grants from the National Eye Institute and the Lucille P. Markey Charitable Trust and by a Searle Scholar's Award.

## References

- Barlow HB, Levick WR (1965) The mechanism of directionally selective units in rabbit's retina. *J Physiol (Lond)* 178:477–504
- Celebrini S, Thorpe S, Trotter Y, Imbert Y (1993) Dynamics of orientation coding in area V1 of the awake primate. *Vis Neurosci* 10:811–825
- DeAngelis GC, Ohzawa I, Freeman RD (1993) Spatiotemporal organization of simple-cell receptive fields in the cat's striate cortex. I. General characteristics and postnatal development. *J Neurophysiol* 69:1091–1117
- DeAngelis GC, Ohzawa I, Freeman RD (1995) Receptive-field dynamics in the central visual pathways. *Trend Neurol Sci* 18:451–458
- Douglas RJ, Koch C, Mahowald M, Martin KAC, Suarez HH (1995) Recurrent excitation in neocortical circuits. *Science* 269:981–985
- Erwin E, Miller KD (1996). Modeling joint development of ocular dominance and orientation maps in primary visual cortex. In: Bower JM (ed) *Computational neuroscience: trends in research 1995*. Academic Press, New York, pp 179–184 Available as <ftp://ftp.keck.ucsf.edu/pub/erwin/CNS95proc.ps.Z>.
- Feidler JC, Saul AB, Murthy A, Humphrey AL (1997) Hebbian learning and the development of direction selectivity: the role of geniculate response timings. *Network* 8:195–214
- Ferster D (1988) Spatially opponent excitation and inhibition in simple cells of the cat visual cortex. *J Neurosci* 8:1172–1180
- Hubel DH, Wiesel TN (1963) Receptive fields of cells in striate cortex of very young, visually inexperienced kittens. *J Neurophysiol* 26:994–1002
- Jones JP, Palmer LA (1987) An evaluation of the two-dimensional Gabor filter model of simple receptive fields in cat striate cortex. *J Neurophysiol* 58:1233–1258
- Kim U, Bal T, McCormick DA (1995) Spindle waves are propagating synchronized oscillations in the ferret LGNd in vitro. *J Neurophysiol* 74:1301–1323
- Maex R (1994) Direction-selective simple cells in cat striate cortex: a modelling study. Leuven University Press, Leuven
- Maex R, Orban GA (1991) Subtraction inhibition combined with a spiking threshold accounts for cortical direction selectivity. *Proc Natl Acad Sci USA* 88:3549–3553
- Mastronarde DN (1983) Correlated firing of cat retinal ganglion cells. I. Spontaneously active inputs to X and Y cells. *J Neurophysiol* 49:303–324
- Mastronarde DN (1983) Correlated firing of cat retinal ganglion cells. II. Responses of X- and Y-cells to single quantal events. *J Neurophysiol* 49:325–349
- McCormick DA, Trent F, Ramoa AS (1995) Postnatal development of synchronized network oscillations in the ferret dorsal lateral geniculate and perigeniculate nuclei. *J Neurosci* 15:5739–5752
- Meister M, Lagnado L, Baylor DA (1995) Concerted signaling by retinal ganglion cells. *Science* 270:1207–1210
- Miller KD (1994) A model for the development of simple cell receptive fields and the ordered arrangement of orientation columns through activity dependent competition between ON- and OFF-center inputs. *J Neurosci* 14:409–441
- Nicholls JG, Martin AR, Wallace BG (1992) *From neuron to brain*. Sinauer, Sunderland, Mass
- Piepbrock C, Ritter H, Obermayer H (1997) The joint development of orientation and ocular dominance: Role of constraints. *Neural Comput* 9:959–970
- Ringach DL, Hawken MJ, Shapley R (1997) Dynamics of orientation tuning in macaque primary visual cortex. *Nature* 387:281–284
- Saul AB, Humphrey AL (1990) Spatial and temporal response properties of lagged and nonlagged cells in cat lateral geniculate nucleus. *J Neurophysiol* 64:206–224
- Saul AB, Humphrey AL (1992) Evidence of input from lagged cells in the lateral geniculate nucleus to simple cells in cortical area 17 of the cat. *J Neurophysiol* 68:1190–1208
- Shevelev IA, Sharaev GA, Lazareva NA, Novikova RV, Tikhomirov AS (1993) Dynamics of orientation tuning in the cat striate cortex neurons. *Neuroscience* 56:865–876
- Somers DC, Nelson SB, Sur M (1995) An emergent model of orientation selectivity in cat visual cortical simple cells. *J Neurosci* 15:5448–5465
- Volgushev M, Vidyasagar TR, Pei X (1995) Dynamics of orientation tuning of postsynaptic potentials in the cat visual cortex. *Vis Neurosci* 12:621–628
- Wimbauer S, Wensich OG, Miller KD, van Hemmen JL (1997) Development of spatiotemporal receptive fields of simple cells: I. Model formulation. *Biol Cybern* 77:453–461
- Wörgötter F, Holt G (1991) Spatiotemporal mechanisms in receptive fields of visual cortical simple cells: A model. *J Neurophysiol* 65:494–510
- Wörgötter F, Niebur E, Koch C (1992) Generation of direction selectivity by isotropic intracortical connections. *Neural Comput* 4:332–340

This article was processed by the authors using the L<sup>A</sup>T<sub>E</sub>X style file *pljour2* from Springer-Verlag.